Chemical Engineering Journal 100 (2004) 79–84

Chemical Engineering Journal

www.elsevier.com/locate/cej

Flow through beds of perfusive particles: effective medium model for velocity prediction within the perfusive media

Bader Albusairi, James T. Hsu*

Department of Chemical Engineering, Lehigh University, Bethlehem, PA 18015, USA

Received 29 May 2003; accepted 13 December 2003

Abstract

The effective medium model is a modified model for flow through beds of perfusive particles. This model accounts for the advantages in the existing models and eliminate most of their disadvantages. This model consists of a perfusive particle surrounded by a hypothetical envelope that has fluid only. This envelope is surrounded by a swarm of perfusive particles with permeability equal to the bed permeability. The analytical solution has been obtained by solving Brinkman's equation in the swarm and the perfusive particle and Navier–Stokes equation for creeping flow in the envelope. This model has proven to converge to the existing models. Where, the proposed model is more general. The validity of this model has been tested through the relation between its parameters, where a relation has been derived through the macroscopic and microscopic force balances on a perfusive bed and a single perfusive particle, respectively. The analysis shows that the result from the effective medium model is in a good agreement with the available experimental data for overall bed permeability.
© 2004 Elsevier B.V. All rights reserved.

Keywords: Perfusive particle; Perfusive packed bed; Velocity profile; Permeability; Effective medium model

1. Introduction

Chemical processes that use porous particles with interconnected pores, i.e., perfusive particles, has emerged as a novel approach to solve the backpressure problems and low efficiency in packed beds such as HPLC, [1–4], also, this approach has show a significant effect in reducing hot spots in exothermic reactors, [5,6] and increasing the effectiveness factor for heterogeneous reactions, [7–10].

The improvement of most of the chemical processes that uses perfusive particles has been justified by Rodrigues et al. [11], through augmented diffusivity, D_{aug}, concept, Eq. (1), where, D_i is effective particle diffusivity and $f(\lambda')$ is defined by Eq. (2) with λ' as particle Peclet number. Where, value of augmented diffusivity increase with increasing amount of flow that pass through the perfusive particle, which indicates less resistance to mass transfer through the particle, i.e., higher efficiency. And since flow through perfusive particles is the major phenomenon that distinguishes perfusive processes from other conventional processes and since it is required to modify other process properties such as augmented diffusivity, overall bed permeability, mobile to particle mass transfer coefficient and dispersion coefficient, then good estimation of the velocity profile internal and external to the perfusive particle would be of great important.

$$D_{aug} = \frac{D_i}{f(\lambda')} \tag{1}$$

$$f(\lambda') = \frac{3}{\lambda'}\left(\frac{1}{\tanh(\lambda')} - \frac{1}{\lambda'}\right) \tag{2}$$

Wheeler [12], was one of the first to discuss flow through porous particle and when it becomes important. Unfortunately, they did not provide a method to estimate intraparticle velocity. In recent decades, intraparticle velocity has been estimated as fraction of the superficial velocity as first attempt, [1,13]. After that, more advanced models have been proposed, [14–16]. Among those models, two major models for predicting the entire velocity profile are of interest. First proposed model is the cell model, Fig. 1A, which has been proposed by Neale et al. [15]. This model is an extension to Happel's model for impermeable particles, [17]. While the second proposed model is the swarm model, Fig. 1B, which has been proposed by Davis and Stone [14]. This model is an extension to Brinkman's model for impermeable particles, [18]. In both of them a second-degree momentum balance has been used and solved analytically, i.e., Brinkman's and Navier–Stokes equations for creeping flow.

Since the convection inside the perfusive particle is the new phenomena under study, then using a good and valid

* Corresponding author. Tel.: +1-610-758-4257; fax: +1-610-758-5851.
E-mail address: jth0@lehigh.edu (J.T. Hsu).

1385-8947/$ – see front matter © 2004 Elsevier B.V. All rights reserved.
doi:10.1016/j.cej.2003.12.004

Nomenclature

b_1	perfusive particle radius
b_2	hypothetical envelope radius
D	diffusivity
k	permeability
P	pressure
r	radial position
R	dimensionless radial position $= r/b_1$
$\boldsymbol{U}$	imposed uniform velocity vector
$\boldsymbol{u}$	velocity vector

Greek letters

β	dimensionless resistance to the flow $= b_1/k^{0.5}$
ε	void fraction $= 1-\phi$
λ	ratio between the envelope and the particle radiuses $= b_2/b_1$
λ'	particle Peclet number $= u_i b_1/(2D_i)$
μ	viscosity
τ	shear stress

Subscript

aug	augmented
e	external
en	envelope
i	internal or inside the perfusive particle

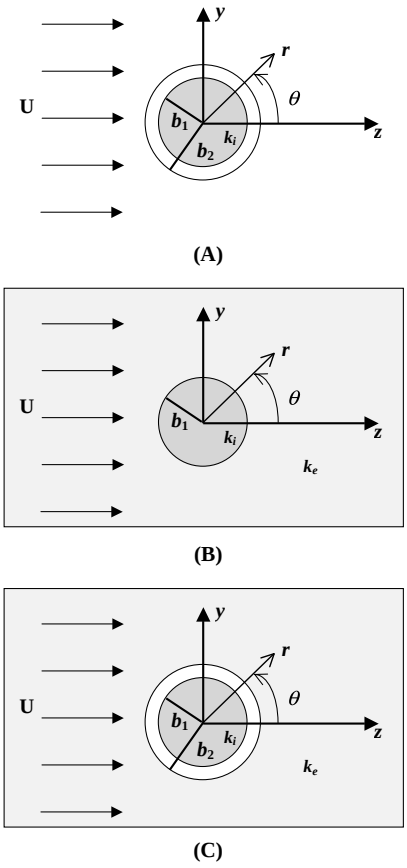

Fig. 1. Schematic draw of the (A) cell model; (B) swarm model; and (C) effective medium model.

model from theoretical and experimental viewpoints would be of great importance. Unfortunately, cell and swarm models have carried the same advantages and disadvantages associated with Happel's and Brinkman's models, respectively. The cell model does not account for the effect of the neighboring particles on the predicted flow. While the swarm model does not account for the flow characteristic around the perfusive particle, it underestimates overall permeability of beds with low porosities, and it is not valid for perfusive beds with porosity less than 0.35 and packed with perfusive particles that have a permeability less than $10^{-3}\ b_1^2$, where b_1 is the perfusive particle radius, [14].

When the perfusive processes have emerged as new technique for protein separation, the cell model was the first and the only advanced flow model to be used, [2]. This model can predict the internal flow inside the perfusive particle very fairly, but it is physically not feasible for the external flow prediction since it has the discontinuity of the velocity profile at the surface of the hypothetical envelope. On the other hand, the swarm model does not have this discontinuity in the velocity profile. But, unfortunately, the region where the swarm model is invalid is the practical region for existing perfusive processes. Thus, a new model is required: (1) to circumvent the major disadvantages of the existing models; and (2) as a tool for comparison with the cell model predictions in the practical region.

In 1974, an effective medium model for impermeable particle that accounted for the major disadvantages of both Happel's and Brinkman's models was proposed [19]. This model has shown a good agreement with the experimental data of impermeable packed beds for both permeability measurements and heat and mass transfer parameters measurements, [19–23]. Also, this model has the potential to be valid in the regions where the swarm one is not valid and the potential to provide complete velocity profile where the cell model does not provide. Therefore, this model will be extended to the case of perfusive particles. First, the proposed effective medium model will be solved using stream function method. Second, the developed model will be compared with the existing models to show that these models are the limiting cases of the proposed effective medium model. Finally, the effect of using perfusive particles on the overall permeability of the perfusive beds will be calculated through the effective medium model, and then it will be compared with an experimental data.

2. Effective medium model

2.1. Model description

The effective medium model, Fig. 1C, is considered to consist of a reference isotropic perfusive spherical particle of

radius b_1 and internal permeability of k_i surrounded by a hypothetical spherical envelope of radius b_2, then both the particle and the envelope are imbedded in an infinite, isotropic, and homogeneous external swarm of perfusive particles of permeability k_e. Far away from the envelope, a uniform, incompressible, creeping, and Newtonian Darcy flow of velocity $\boldsymbol{U}$ occurs due to the pressure drop across the bed length. The radius of the hypothetical envelope will be determined by the porosity of the bed, ε_e, where the envelope volume is considered as the bed void associated with the perfusive particle. Accordingly, the envelope radius, b_2, will be calculated by Eq. (3), where ϕ is the perfusive particles fraction in the bed.

$$\lambda = \frac{b_2}{b_1} = \phi^{-1/3} = (1-\varepsilon_e)^{-1/3} \tag{3}$$

2.2. Governing equations

The imposed uniform flow is considered in the z-direction only, i.e., $\boldsymbol{U} = U\boldsymbol{\delta}_z$, where $\boldsymbol{\delta}_z$ is the unit direction vector in the z-direction. The flow field in the envelope is governed by the Navier–Stokes equation, while the flow field in the external swarm of perfusive particles and the reference perfusive particle is governed by Brinkman's equation. Thus, the governed equations are:

$$-\frac{\mu}{k_e}\boldsymbol{u}_e + \mu\nabla^2\boldsymbol{u}_e = \nabla P_e, \qquad r > b_2 \tag{4}$$

$$\mu\nabla^2\boldsymbol{u}_{en} = \nabla P_{en}, \qquad b_1 < r < b_2 \tag{5}$$

$$-\frac{\mu}{k_i}\boldsymbol{u}_i + \mu\nabla^2\boldsymbol{u}_i = \nabla P_i, \qquad r < b_1 \tag{6}$$

$$\nabla\cdot\boldsymbol{u}_j = 0, \qquad j = e, en, i \tag{7}$$

where $\boldsymbol{u}$ and P are the velocity vector and the pressure, respectively. And the subscripts e, en, and i refers to external, envelope, and inside regions, respectively.

The boundary conditions that shall be used must represent the actual physical system. Accordingly, the continuity of the pressure, the flow vector, and the shear tensor throughout the proposed model must be satisfied. Therefore, the appropriate boundary conditions are shown below, where $\tau_{r\theta}$ is the tangential shear stress.

$$\boldsymbol{u}_e = \boldsymbol{U}, \qquad P_e = P_o - \frac{\mu}{k_e}\boldsymbol{U}\cdot\boldsymbol{r}, \qquad r = |r| \to \infty \tag{8}$$

$$\boldsymbol{u}_e = \boldsymbol{u}_{en}, \qquad P_e = P_{en}, \qquad \tau_{r\theta,e} = \tau_{r\theta,en}, \qquad r = b_2 \tag{9}$$

$$\boldsymbol{u}_{en} = \boldsymbol{u}_i, \qquad P_{en} = P_i, \qquad \tau_{r\theta,en} = \tau_{r\theta,i}, \qquad r = b_1 \tag{10}$$

$$\boldsymbol{u}_i = \text{finite}, \qquad P_i = P_o, \qquad r = 0 \tag{11}$$

3. Results and discussion

3.1. Velocity expressions

Stream function, ψ, method, [15,24], has been used to solve the mathematical governed equations. The major obtained expressions are:

$$\psi_e = \frac{U b_1^2}{2\beta_e^2}\left[\frac{A_1}{\beta_e R} + B_2(\beta_e R)^2 + C_1\left(1-\frac{1}{\beta_e R}\right)\exp(\beta_e R) + D_1\left(1+\frac{1}{\beta_e R}\right)\exp(-\beta_e R)\right](\sin\theta)^2 \tag{12}$$

$$\psi_{en} = \frac{U b_1^2}{2}\left[\frac{A_2}{R} + B_2 R + C_2 R^2 + D_2 R^4\right](\sin\theta)^2 \tag{13}$$

$$\psi_i = \frac{U b_1^2}{2\beta_i^2}\left[\frac{A_3}{\beta_i R} + B_3(\beta_i R)^2 + C_3\left(\frac{\cosh(\beta_i R)}{\beta_i R} - \sinh(\beta_i R)\right) + D_3\left(\frac{\sinh(\beta_i R)}{\beta_i R} - \cosh(\beta_i R)\right)\right](\sin\theta)^2 \tag{14}$$

where $\beta_e = b_1/k_e^{0.5}$, $\beta_i = b_1/k_i^{0.5}$, $R = r/b_1$, and As, Bs, Cs, and Ds are constants determined by the boundary conditions. The corresponding velocity components can be found by using Eq. (15) for the radial component of the velocity vector and Eq. (16) for the tangential one. Then, the resulted expressions for velocity vectors are used in Eqs. (4)–(6) to obtain the expressions for P_e, P_{en}, and P_i, respectively. The constants expressions are shown in Appendix A.

$$u_r = \frac{-1}{b_1^2 R^2\sin(\theta)}\frac{\partial\psi}{\partial\theta} \tag{15}$$

$$u_\theta = \frac{1}{b_1^2 R\sin(\theta)}\frac{\partial\psi}{\partial R} \tag{16}$$

$$P_e = \frac{-1}{2}\frac{\mu\beta_e U}{b_1}\left(\frac{A_1}{\beta_e^2 R^2} - 2B_1\beta_e R\right)\cos(\theta) + P_o \tag{17}$$

$$P_{en} = \frac{-\mu U}{b_1}\left(\frac{B_2}{R^2} + 10D_2 R\right)\cos(\theta) + P_o \tag{18}$$

$$P_i = \frac{\mu\beta_i^2 U}{b_1}B_3 R\cos(\theta) + P_o \tag{19}$$

After this point, all constants that are not function of β_i, β_e, and λ will be replaced by their constant value in the mathematical expressions.

3.2. Limiting cases

Effective medium model can be considered as a combination of the swarm and the cell models and as modification to

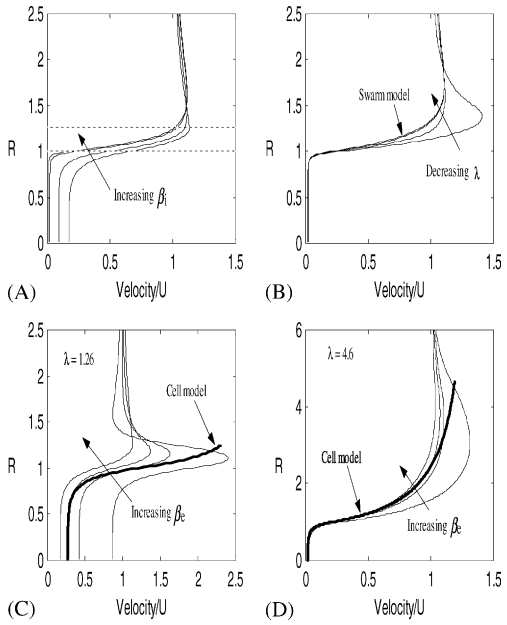

Fig. 2. (A) Velocity profiles for the effective medium model as β_i increased; (B) convergence of the velocity profiles if the effective medium model to velocity profile of the swarm model as λ decreased; comparison between cell model velocity profiles and the effective medium model velocity profiles at (C) low λ (λ = 1.26) and (D) high λ (λ = 4.6).

the original effective medium model for impermeable particles. Therefore, this model should represent all of them. Accordingly, Fig. 2 has been constructed. In Fig. 2A, it can be noticed that as $\beta_i \to \infty$ ($k_i \to 0$), the proposed model represents the original effective medium model for impermeable particles. In Fig. 2B, when $\lambda \to 1$ the proposed model represents the swarm model for any value of β_i and β_e.

In the case of convergence to the cell model, a main obstacle that shall be faced is the difference in the physical system, where the cell model does not predict beyond $R = \lambda$, while the effective medium model predict. Therefore, Fig. 2C and D had been constructed. Both of the figures show that the effective medium model may present the cell model for a specific combination of λ and β_e. Also, they showed that the effective medium model represents the cell model more accurately as the value of λ increases.

Thus, the effective medium model can be considered as the most general model for velocity prediction in systems enclosed of permeable particles as well as impermeable ones. Where, it can represent all the proposed models yet except for the cell model at low values of λ and this due to the geometry of the proposed models and their boundary conditions at $R = \lambda$.

3.3. Overall perfusive bed permeability

The prediction of overall perfusive bed permeability, k_e, is practically important because it gives a measure to how the perfusive bed differs from the traditional one, and because it gives us a tool to verify the proposed models experimentally. To estimate the perfusive bed permeability, k_e, in terms of perfusive particle permeability, k_i, and bed porosity, ε_e, the following procedure has been adopted from Davis and Stone [14].

Overall perfusive bed permeability, k_e, relates to the imposed uniform velocity and the pressure gradient by Darcy's law, Eq. (20). Applying a macroscopic force balance on the bed will give an expression for the drag force per particle, $\boldsymbol{F}_D$, Eq. (21). Then $u_{en,\,r}$ at $R = 1$ from the effective medium model results has been used to calculate the magnitude of the drag force per particle, Eq. (22).

$$\boldsymbol{U} = -\frac{k_e}{\mu}\nabla P \tag{20}$$

$$\boldsymbol{F}_D = -\nabla P\left(\frac{4\pi b_1^3}{3\phi}\right) \tag{21}$$

$$\begin{aligned}\boldsymbol{F}_D &= -2\pi b_1^2\int_0^{\pi}[(p+\tau_{rr})\cos\theta - \tau_{r\theta}\sin\theta]_{r=b_1}\sin\theta\, d\theta \\ &= 4\pi b_1 \mu U B_2\end{aligned} \tag{22}$$

Finally, combining Eqs. (20)–(22), will yield a relation between β_i, β_e, and $\lambda = \phi^{-1/3} = (1-\varepsilon_e)^{-1/3}$, Eq. (23). This relation and similar ones obtained for the swarm and cell models, [14], are plotted in Fig. 3 for comparison.

$$B_2 - \frac{1}{3}\beta_e^2\lambda^3 = 0 \tag{23}$$

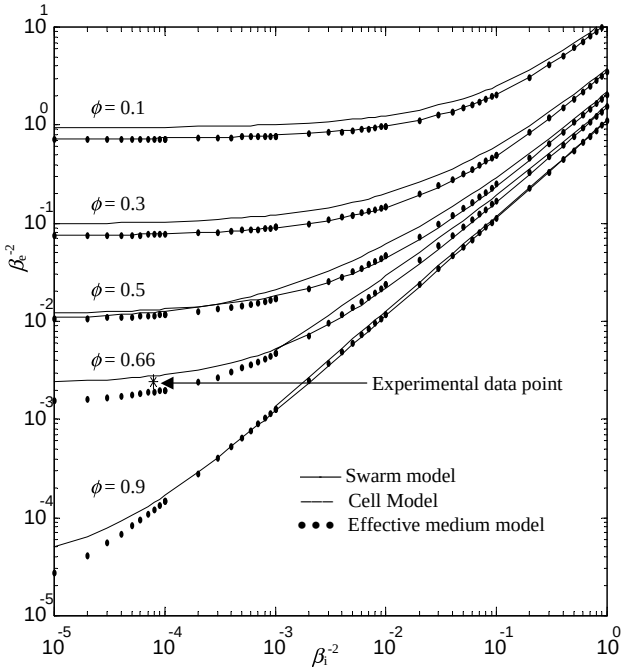

Fig. 3. Overall bed permeability as function of the internal perfusive particle permeability for several values of bed porosity: (- - -) the cell model; (—) the swarm model; (●●●) the effective medium model; (✳) experimental data point extracted from Pfeiffer et al. [25] and Rodrigues et al. [26].

From Fig. 3, at low β_i the three models predict almost the same values of β_e for all values of ϕ. On the other hand, at high β_i the predictions of the cell model and the effective medium model of β_e values are identical at low ϕ values, but they are differ at high ϕ values. This proves that the effective medium model converge to the cell model for high porous beds (high λ).

On the experimental side, Pfeiffer et al. [25], has reported that the permeability of a perfusive particle called POROS is equal to $7.89 \times 10^{-15}\,m^2$. While, Rodrigues et al. [26], has reported that using the same kind of particle with diameter equal to 20 μm in a perfusive bed that has a porosity equal to 0.34 will result in overall bed permeability equal to $2.42 \times 10^{-13}\,m^2$. Fig. 3 shows where this experimental data is located in the chart of β_e versus β_i for $\phi = 0.66$ with respect to the predictions of cell and effective medium models. As observed the single experimental data is located within the range of the prediction of both models.

3.4. Comparison of the proposed effective medum model with cell and swarm models

All the previous observations indicate that the new model predict the overall bed permeability as accurate as the existing models, but it is not necessary that all of them predict the same heat and transfer parameters as found recently, [21].

According to the derivation, the effective medium model has account for flow characteristics that is not totally covered by the existing models. Also, from the results, it was found that the effective medium model is valid in the region where the swarm model is not and it has a continuous external velocity profile, in which the cell model has not. Finally, the effective medium model for impermeable particles has shows a good result in heat and mass transfer rates as well as in the prediction of permeability, [19–23]. Therefore, it is a better candidate for predicting transport phenomena parameters in perfusive systems.

4. Conclusion

New effective medium model for predicting the flow in a perfusive bed has been developed and solved analytically by using the stream function. The new model accounts for the characteristics of the flow around the perfusive particle as well as the effect of the neighboring particles. The new model consists of three regions, the internal region that accounts for the perfusive particle, the envelope region that accounts for the bed porosity, and the external region that accounts for the swarm of the perfusive particles. The new model has been proven to converge to the two existing models when the porosity is set to its limits.

Experimentally and theoretically it was proven that the new effective medium model predict the overall permeability as accurate as the existing models. On the other hand, it has many advantages over the existing models, and it can be used, in the future, as a better model in heat and mass transfer problems.

Appendix A. Constant of integration expressions

$$A_1 = -2\beta_e^3\lambda^3 + 20\beta_e\lambda^3 D_2 + 2\beta_e B_2 \tag{A.1}$$

$$B_1 = -1 \tag{A.2}$$

$$C_1 = A_3 = C_3 = 0 \tag{A.3}$$

$$B_3 = \frac{-1}{\beta_i^2}(B_2 + 10D_2) \tag{A.4}$$

$$D_1 = \frac{6}{\delta_1}[2\beta_e^3\lambda^3 + \beta_e^3 A_2 - 2\beta_e B_2 + (\beta_e^3\lambda^5 - 20\beta_e\lambda^3)D_2] \times \exp(\beta_e\lambda) \tag{A.5}$$

$$\delta_1 = 6 + 3\beta_e^2\lambda^2 + 6\beta_e\lambda + \beta_e^3\lambda^3 \tag{A.6}$$

$$D_3 = \frac{-6\beta_i^3(A_2 + D_2)}{(6 + \beta_i^3)\beta_i\cosh(\beta_i) - (6 + 3\beta_i^2)\sinh(\beta_i)} \tag{A.7}$$

$$\begin{aligned} A_2 = {} & (\beta_e^2[3 + \beta_e\lambda])^{-1}\{-\lambda(3\beta_e^2\lambda + 4\beta_e + \beta_e^3\lambda^2)B_2 \\ & -\lambda(6 + 3\beta_e^2\lambda^2 + 6\beta_e\lambda + \beta_e^3\lambda^3)C_2 \\ & -\lambda(-60\lambda^2 + 3\beta_e^2\lambda^4 - 20\beta_e\lambda^3 + \beta_e^3\lambda^5)D_2 \\ & -\lambda(6\beta_e\lambda + 3\beta_e^3\lambda^3 + 9\beta_e^2\lambda^2 + 6)\} \end{aligned} \tag{A.8}$$

$$\begin{aligned} B_2 = {} & \frac{6\beta_i^2}{\delta_2}\{[((6\lambda + 15\lambda^4 - 6\lambda^6)\beta_e^3 + (6 + 15\lambda^3 - 21\lambda^5)\beta_e^2 \\ & -45\beta_e\lambda^4 - 45\lambda^3)\beta_i^2 + (15\lambda + 30\lambda^4)\beta_e^3 \\ & +(15 + 30\lambda^3)\beta_e^2]\sin h(\beta_i) - [((\lambda + 5\lambda^4 - 6\lambda^6)\beta_e^3 \\ & +(1 + 5\lambda^3 - 21\lambda^5)\beta_e^2 - 45\beta_e\lambda^4 - 45\lambda^3)\beta_i^2 \\ & +(15\lambda + 30\lambda^4)\beta_e^3 + (15 + 30\lambda^3)\beta_e^2]\beta_i\cos h(\beta_i)\} \end{aligned} \tag{A.9}$$

$$\begin{aligned} C_2 = {} & \frac{-3}{\delta_2}\{[15[(\lambda + \lambda^3)\beta_e^3 + (1 - \lambda^2)\beta_e^2]\beta_i^4 \\ & +((72\lambda + 30\lambda^3 - 12\lambda^6)\beta_e^3 + (72 - 30\lambda^2 - 42\lambda^5)\beta_e^2 \\ & -90\beta_e\lambda^4 - 90\lambda^3)\beta_i^2 + 90\beta_e^3\lambda + 90\beta_e^2]\sinh(\beta_i) \\ & -[[(3\lambda + 5\lambda^3 - 8\lambda^6)\beta_e^3 + (3 - 5\lambda^2 - 28\lambda^5)\beta_e^2 \\ & -60\beta_e\lambda^4 - 60\lambda^3]\beta_i^4 + ((42\lambda + 30\lambda^3 - 12\lambda^6)\beta_e^3 \\ & +(42 - 30\lambda^2 - 42\lambda^5)\beta_e^2 - 90\beta_e\lambda^4 - 90\lambda^3)\beta_i^2 \\ & +90\beta_e^3\lambda + 90\beta_e^2]\beta_i\cosh(\beta_i)\} \end{aligned} \tag{A.10}$$

$$\begin{aligned} D_2 = {} & \frac{3\beta_e^2\beta_i^2}{\delta_2}\{[3((\lambda + \lambda^3)\beta_e - \lambda^2 - 1)\beta_i^2 \\ & +6((\lambda - \lambda^4)\beta_e - \lambda^3 + 1)]\sinh(\beta_i) \\ & -[((\lambda + 3\lambda^3 - 4\lambda^4)\beta_e - 4\lambda^3 - 3\lambda^2 + 1)\beta_i^2 \\ & +6((\lambda - \lambda^4)\beta_e - \lambda^3 + 1)]\beta_i\cosh(\beta_i)\} \end{aligned} \tag{A.11}$$

$$\delta_2 = [\delta_{21}\beta_i^4 + \delta_{22}\beta_i^2 + 270\beta_e^2 + 270\beta_e^3\lambda]\sinh(\beta_i) - [\delta_{23}\beta_i^4 + \delta_{24}\beta_i^2 + 270\beta_e^2 + 270\beta_e^3\lambda]\beta_i\cosh(\beta_i) \quad (A.12)$$

$$\delta_{21} = (-24 + 45\lambda - 30\lambda^3 + 9\lambda^5)\beta_e^3 + (45 - 90\lambda^2 + 45\lambda^4)\beta_e^2 + 180\lambda^3\beta_e \quad (A.13)$$

$$\delta_{22} = (-60 + 216\lambda - 60\lambda^3 - 6\lambda^6)\beta_e^3 + (216 - 180\lambda^2 - 36\lambda^5)\beta_e^2 - 270\lambda^4\beta_e - 270\lambda^3 \quad (A.14)$$

$$\delta_{23} = (-4 + 9\lambda - 10\lambda^3 + 9\lambda^5 - 4\lambda^6)\beta_e^3 + (9 - 30\lambda^2 + 45\lambda^4 - 24\lambda^5)\beta_e^2 + (180\lambda^3 - 180\lambda^4)\beta_e - 180\lambda^3 \quad (A.15)$$

$$\delta_{24} = (-60 + 126\lambda - 60\lambda^3 - 6\lambda^6)\beta_e^3 + (126 - 180\lambda^2 - 36\lambda^5)\beta_e^2 + 270\lambda^4\beta_e + 270\lambda^3 \quad (A.16)$$

References

[1] N.B. Afeyan, N.F. Gordon, I. Mazsaroff, L. Varady, S.P. Fulton, Y.B. Yang, F.E. Regnier, Flow-through particles for the high-performance liquid chromatographic separation of biomolecules: perfusion chromatography, J. Chromatogr. 519 (1) (1990) 1–29.

[2] G. Carta, M.E. Gregory, D.J. Kirwan, H.A. Massaldi, Chromatography with permeable supports: theory and comparison with experiments, Sep. Technol. 2 (2) (1992) 62–72.

[3] A.I. Liapis, M.A. McCoy, Theory of perfusion chromatography, J. Chromatogr. 599 (1–2) (1992) 87–104.

[4] A.E. Rodrigues, J.C. Lopes, Z.P. Lu, J.M. Loureiro, M.M. Dias, Importance of intraparticle convection in the performance of chromatographic processes, J. Chromatogr. 590 (1) (1992) 93–100.

[5] J.C. Lopes, M.M. Dias, V.G. Mata, A.E. Rodrigues, Flow field and non-isothermal effects on diffusion, convection, and reaction in permeable catalysts, Ind. Eng. Chem. Res. 34 (1) (1995) 148–157.

[6] A.E. Rodrigues, R.M. Quinta Ferreira, Effect of intraparticle convection on the steady-state behavior of fixed-bed catalytic reactors, Chem. Eng. Sci. 45 (8) (1990) 2653–2660.

[7] A. Nir, L.M. Pismen, Simultaneous intraparticle forced convection, Chem. Eng. Sci. 32 (1) (1977) 35–41.

[8] A. Nir, Simultaneous intraparticle forced convection, diffusion and reaction in a porous catalyst. II. Selectivity of sequential reactions, Chem. Eng. Sci. 32 (8) (1977) 925–930.

[9] A.E. Rodrigues, Z.P. Lu, J.C.B. Lopes, M.M. Dias, A.M. Silva, The effect of intraparticle convection on conversion in heterogeneous isothermal fixed-bed reactors with large-pore catalysts for first-order reactions, Chem. Eng. J. Biochem. Eng. 54 (1) (1994) 41–50.

[10] A. Leitao, A. Rodrigues, Catalytic processes using "large-pore" materials: effects of the flow rate and operating temperature on the conversion in a plug-flow reactor for irreversible first-order reactions, Chem. Eng. J. Biochem. Eng. 60 (1–3) (1995) 111–116.

[11] A.E. Rodrigues, B.J. Ahn, A. Zoulalian, Intraparticle-forced convection effect in catalyst diffusivity measurements and reactor design, AIChE 28 (4) (1982) 541–546.

[12] A. Wheeler, Reaction rates and selectivity in catalyst pores, Adv. Catal. 3 (1951) 250–337.

[13] H. Komiyama, H. Inoue, Effects of intraparticle convective flow on catalytic reactions, J. Chem. Eng. Jpn. 7 (4) (1974) 281–286.

[14] R.H. Davis, H.A. Stone, Flow through beds of porous particles, Chem. Eng. Sci. 48 (23) (1993) 3993–4005.

[15] G. Neale, N. Epstein, W. Nader, Creeping flow relative to permeable spheres, Chem. Eng. Sci. 28 (10) (1973) 1865–1874.

[16] K. Nandakumar, J.H. Masliyah, Laminar flow past a permeable sphere, Can. J. Chem. Eng. 60 (2) (1982) 202–211.

[17] J. Happel, Viscouse flow in multiparticle systems: slow motion of fluids relative to beds of spherical particles, AIChE 4 (2) (1958) 197–201.

[18] H.C. Brinkman, A calculation of the viscous force exerted by a flowing field on a dense swarm of particles, Appl. Sci. Res. A1 (1947) 27–34.

[19] G.H. Neale, W.K. Nader, Prediction of transport processes within porous media: creeping flow relative to a fixed swarm of spherical particles, AIChE 20 (3) (1974) 530–538.

[20] G.H. Neale, W.K. Nader, Prediction of transport processes within porous media: diffusive flow processes within a homogeneous swarm of spherical particles, AIChE 19 (1) (1973) 112–119.

[21] W. Wang, A.S. Sangani, Nusselt number for flow perpendicular to arrays of cylinders in the limit of small Reynolds and large Peclet numbers, Phys. Fluid 9 (6) (1997) 1529.

[22] T.L. Dodd, D.A. Hammer, A.S. Sangani, D.L. Koch, Numerical simulations of the effect of hydrodynamic interactions on diffusivities of integral membrane proteins, J. Fluid Mech. 293 (1995) 147.

[23] Y. Li, C.-W. Park, Effective medium approximation and deposition of colloidal particles in fibrous and granular media, Adv. Colloid Interface Sci. 87 (1) (2000) 1–74.

[24] R.B. Bird, W.E. Stewart, E.N. Lightfoot, Transport Phenomena, first ed., Wiley, New York, 1960, p. 780.

[25] J.F. Pfeiffer, J.C. Chen, J.T. Hsu, Permeability of gigaporous particles, AIChE 42 (4) (1996) 932–939.

[26] A.E. Rodrigues, J.M. Loureiro, C. Chenou, M.R. de la Vega, Bioseparations with permeable particles, J. Chromatogr. B 664 (1) (1995) 233–240.